Transactions, SMiRT-22
San Francisco, California, USA - August 18-23, 2013
Division II Fracture Mechanics

CONSIDERATION OF CONSTRAINT IN PLASTICITY ENHANCEMENT FOR COMBINED PRIMARY AND SECONDARY STRESSES ON CRACK DRIVING FORCE

Peter James[1], Dennis Hooton[2] and Peter Budden[3]

[1] Technical Services, AMEC, Walton House, Risley, Warrington, UK (peter.james2@amec.com)
[2] Technical Services, AMEC, Walton House, Risley, Warrington, UK
[3] EDF Energy, Barnett Way, Barnwood, Gloucester, UK

ABSTRACT

To assess the criticality of a crack-like defect in a component, it is necessary to consider the value of crack driving force, which can then be compared to a representative material's fracture toughness. The value of the crack driving force used can be determined from elastic-plastic finite element analysis or, more conveniently, by making use of simplified methods such as those contained in the R6 assessment procedure. These assessments must take into account all applied loads, including the combined effect of primary and secondary loads acting to open the crack. A range of methods are currently available within R6 to describe how these primary and secondary stresses combine, with further approaches suggested for the next revision. Recently developed was an approach by James, termed the "g-function", to consider the interaction of primary and secondary stresses in typical components. This paper reconsiders how the estimate of the plasticity interaction term, $g()$, which is used in the g-function method can be adapted to different geometries. By considering a range of geometries, with differing constraint levels, some insight into the value of these terms has been provided, which in turn allows further confidence in the use of $g()$. The work has shown that the finite element estimates of $g()$ considered in this paper follow the same trends as provided by James and that the use of the constraint term, Q, in the estimate of $g()$ can provide improved results. However, in practice, this benefit may be small as the influence of the primary stress will be significant for these cases.

INTRODUCTION

To assess the criticality of a crack-like defect in a component, it is necessary to consider the value of crack driving force, which can then be compared to a representative material's fracture toughness. The value of the crack driving force used can be determined from elastic-plastic finite element analysis or, more conveniently, by making use of simplified methods such as those contained in the R6 assessment procedure [1]. These assessments must take into account all applied loads, including the combined effect of primary and secondary loads acting to open the crack. For pressurised plant components, primary loads arise from applied forces such as internal pressure; secondary loads typically arise from weld residual stresses and thermal stresses.

A range of methods are currently available within R6 [1] to describe how these primary and secondary stresses combine, with further approaches suggested for the next revision, although these are not considered here. Each of these methods has different levels of associated conservatism which can be significant in certain circumstances. Recently, further estimates of this interaction based upon the *V* factor in R6 have been proposed by a number of authors. In particular, approaches of Song et al. [2] and Ainsworth [3] have been developed to consider the effect of elastic follow-up on the magnitude of the *V* factor. Also developed recently was an approach by James [4], termed the "g-function", to consider the interaction of primary and secondary stresses in typical structures with thermally induced through wall bending and biaxial primary loading. All of these approaches have noted the similar form of the *V* interaction term to the curve describing the R6 Option 2 failure assessment diagram (FAD), therefore also allowing materials dependence in this interaction term, but differ in their application. In this present paper, only the g-function approach is considered further.

This paper reconsiders how the estimate of the plasticity interaction term, $g()$, which is used in the g-function method, can be adapted to different geometries. More specifically, two constants, termed A and B in [4] are considered that provide a means to fit finite element estimates of $g()$. These two constants were initially included to maintain conservatism when compared to finite element analyses by controlling both the magnitude of the increase of $g()$ above unity, and in defining the skeletal point for $g()$, respectively. It is by considering a range of geometries, with differing constraint levels, that some insight into the value of these terms has been provided, which in turn allows further confidence in the use of $g()$.

The geometries used in the analyses include a Centre Cracked Plate in Tension (CCPT), a Double Edge Notched plate in Tension (DENT), a Single Edge Notched plate in Tension (SENT) and a Single Edge Notched plate under Bending (SENB), each with a shallow and deep crack. For each of these geometries, both combined primary and thermally induced secondary stresses are applied and $g()$ evaluated from the finite element analyses, $g()_{FE}$. The value of $g()_{FE}$ is then used to identify the idealised values for A and B. An estimate of constraint is also provided for each geometry and loading condition by way of the constraint parameter, Q.

BACKGROUND

This section provides a review of the generalised R6 approach for combined loading before progressing to consider two plasticity correction terms used to define how the primary and secondary stresses interact. The two plasticity correction terms are: the ξ term, as a function of both primary and secondary stresses, contained within the current Complex R6 V-Factor Method [1]: and the $g()$ term in the g-Function method [4], which provides a simpler approach.

Determination of the Assessment Point

A conventional R6 assessment considers the criticality of a defect when calculating the elastic stress intensity factors and plotting assessment points on a FAD. The position of the assessment point is defined by the parameters L_r and K_r, where L_r defines the magnitude of applied primary load and is determined from:

$$L_r = \frac{P}{P_L} = \frac{\sigma_{ref}^{p}}{\sigma_y} \tag{1}$$

where P is the applied load, P_L is the plastic limit load for the structure considered and includes the effect of the defect, σ_{ref}^{p} is the primary reference stress and σ_y is the material's 0.2% proof stress. The K_r parameter is given by:

$$K_r = \frac{\left(K_I^P + VK_I^S\right)}{K_{mat}} \tag{2}$$

where K_I^p and K_I^s are the elastic stress intensity factors for primary and secondary stresses respectively and K_{mat} is the material's fracture toughness. Different estimates for the plasticity interaction term, V, are provided in R6, some of which are outlined below. When the assessment point, (L_r, K_r), is plotted on the FAD, defined by a plot of $f(L_r)$ versus L_r together with a material dependent cut-off, $L_r = L_r^{max}$, the component is assumed to have "failed" if the point lies outside the area of the

plot. The definition of the FAD function f is provided by a selection of Options, ranging from Option 1 to Option 3. The Option 1 FAD is both material and geometry independent and is given by Equation (3); the Option 2 FAD is material dependent and geometry independent and is provided by Equation (4); and the Option 3 FAD is both material, geometry and loading dependent and can be obtained from finite element analyses for the determination of the elastic-plastic primary stress intensity factor as in Equation (5).

$$f_1(L_r) = \left[0.3 + 0.7e^{-0.6L_r^6}\right]\left[1 + 0.5L_r^2\right]^{-0.5} \tag{3}$$

$$f_2(L_r) = \left[\frac{E\varepsilon^p_{ref}}{\sigma^p_{ref}} + \frac{0.5\left(\sigma^p_{ref}/\sigma_y\right)^2}{E\varepsilon^p_{ref}/\sigma^p_{ref}}\right]^{-1/2} \tag{4}$$

$$f_3(L_r) = \frac{K_I^p}{K_J^p} \tag{5}$$

where E is the material's Young's modulus, ε^p_{ref} is the strain corresponding to σ^p_{ref}, as defined by the material's true stress-true strain curve, and $K_J^p = \sqrt{EJ^p/(1-\nu^2)}$ is the elastic-plastic primary stress intensity factor, with J^p the value of the *J*-integral for the primary loading alone.

Look-Up Table Definition of ξ

Under the Complex R6 *V*-Factor Method, the estimation of V is provided by:

$$V = \frac{K_J^s}{K_I^s}\xi \tag{6}$$

where $K_J^s = \sqrt{EJ^s/(1-\nu^2)}$ is the elastic-plastic secondary stress intensity factor for the secondary loads alone, and ξ is provided by look-up tables in R6. These tables are given in terms of L_r and the parameter $K_J^s/\left(K_I^p/L_r\right)$. These tables were simply defined from the ψ and φ tables used in defining ρ in the R6 Complex ρ-Factor Method and, as such, they lead to the same result for both Complex V and ρ approaches when considering combined primary and secondary loadings. As has been noted above, it has been shown, however, that these methods can be overly conservative. This has led to the development of a further method which uses $g()$ to quantify the plasticity interaction.

Modified Option 2 FAD Definition of g()

A further method to determine the V-Factor has been defined [4] as below.

$$V = \frac{K_J^s}{K_I^s} f(L_r) g(\,) \tag{7}$$

where $g()$ is provided by Equations (8) to (10) below.

$$g(\ ) = \left[\frac{E\varepsilon_{ref}^{mod}}{\sigma_{ref}^{mod}} + \frac{A\left(\sigma_{ref}^{mod} / \sigma_y\right)^2}{E\varepsilon_{ref}^{mod} / \sigma_{ref}^{mod}} \right]^{-1/2} \tag{8}$$

$$A = -\frac{\sigma^p{}_{in\_plane}}{1.25 \times \bar{\sigma}^p{}_{mises}} \tag{9}$$

$$\sigma_{ref}^{mod} = L_r \sigma_y / B = L_r \sigma_y / 1.25 \tag{10}$$

where ε_{ref}^{mod} is the strain corresponding to σ_{ref}^{mod} as defined by the material's stress-strain curve, $\sigma_{in\_plane}^{p}$ is the remotely applied in-plane primary stress and $\bar{\sigma}_{mises}^{p}$ is the von Mises stress defined from the remotely applied primary loads.

Possible Link of g() to Crack-Tip Constraint

It is noted that the form of $g()$ presented in Equation (8) is based on an Option 2 FAD and, as such, captures the differences seen when using different materials, but not from different geometries. The A term was found to provide conservative comparisons of the effective enhancement above unity for $g()$. As such it captures the enhanced combination of stresses under small-scale yielding before the secondary stress is removed through plastic redistribution. However, this enhancement may not be the same for all geometries, although Equation (9) does appear to be conservative [4, 5]. The form of A provided in Equation (9) was found from fitting estimates of $g()$ for an external fully circumferentially cracked cylinder, where it was also seen to depend on different combinations of hoop and axial stress. However, as Equation (9) uses a simplified estimate of the tri-axial stress state being applied to the cracked geometry, it is also possible that the A term might be linked to a measure of constraint, Q, where Q is determined from the normalised deviation of the stress field from an idealised stress field (with in-plane loading and small-scale yielding).

This difference will be affected by a number of factors including geometry, loading type and crack depth, as well as residual stress. As constraint provides a correction to the J-controlled definition of a stress field, and it is the stress field which determines the level of secondary stress redistribution, it stands to reason that constraint, geometric or otherwise, must also effect how a secondary stress field is redistributed.

It has also been noted that constraint has an effect on the shape of the FAD [6], which is also included in Section III.7 of R6 [1]. The shape of the constraint-modified FAD shares many similarities to that of $g()$: it follows the normal failure assessment curve under elastic failure conditions and is seen to increase above unity under small-scale yielding. The behaviour is somewhat different beyond gross yielding, but this may be expected as $g()$ captures the removal of secondary stresses whereas the constraint modified FAD has to still remain applicable to primary loads. However, of note is that the perceived enhancement above unity in $g()$ under small-scale yielding is also observed when accounting for constraint.

It is also noted that the constraint modified FAD approach in [1] uses a normalised measure of constraint effects, termed the biaxiality ratio, β, which can be expressed as in Equation (11) below.

$$\beta = Q / L_r \tag{11}$$

Under elastic conditions, β is used to relate the elastic stress intensity factor to the elastic T stress measure of constraint, as Q is related to T under such conditions.

The aim of the work presented here is to consider differently constrained geometries to see if a link between A and constraint, either in terms of Q or β, does indeed exist. The range of geometries and broad scope of the work might also help to provide guidance on the value of the B term.

FINITE ELEMENT ANALYSES

This section provides a review of the finite element analyses performed to define $g()_{FE}$ and corresponding estimates of Q. Where required, additional information is provided on the analyses of the Modified Boundary Layer (MBL) model used to define the idealised reference stress field when estimating Q.

Geometries

The geometries considered in this analyses include CCPT, DENT, SENT and SENB test specimens, each with a shallow and deep crack under plane strain conditions. Two cracked meshes, representing two crack depths, were created using ABAQUS 6.9 [7] with the boundary conditions and applied loading modified to allow each geometry to be realised. The basic two-dimensional mesh used in the analyses, which represents half the model for the SENT and SENB geometries and a quarter model for the DENT and CCPT geometries, was 50 mm wide (w) and 100 mm long (l). The two crack depths (a) used are 5 mm ($a/w = 0.1$) and 25 mm ($a/w = 0.5$), which relate to shallow and deep cracks. Note that, for the DENT, the boundary condition meant that there were two symmetrical cracks of depth a and w represents the half-wall thickness. Likewise, for the CCPT geometry, a is the semi-crack length and w represents the half-plate thickness.

For accuracy when providing an estimate of constraint, a very refined mesh was used at the crack tip and can be seen in Figure 1. The same focused mesh was used for both crack depths. Crack tip node degeneracy and mid-side node positions were also modified for both elastic and elastic-plastic conditions to account for crack tip blunting. For accurate detailing of the stress field the smallest element closest to the crack tip was 0.01 mm long. All models were created using ABAQUS CAE [7] and comprised two dimensional (2D) plane strain reduced integration quadratic elements (ABAQUS type CPE8R) under small displacement assumptions.

To provide an estimate of crack tip constraint, a MBL model was used when defining the reference stress field. The model was sized such that the smallest element closest to the crack tip was 0.01 mm long, thus matching the finite element models of the main geometries, and the radius of the model was 1000 mm. The large size of the model was to ensure small-scale yielding conditions under all applied loads.

Material

The material used had a Young's modulus, E, of 300,000 MPa, a Poisson's ratio, ν, of 0.296 and a coefficient of thermal expansion, α, of 1.46 x10^{-5} $^{o}C^{-1}$. The material used had plastic properties defined from the Ramberg Osgood fit shown in Equation (12), where the material's 0.2% proof stress, $\sigma_y = \sigma_{0.2}$, was taken as 300 MPa and three different values of n (5, 7.5 and 10), the strain hardening component, were used.

$$\varepsilon = \frac{\sigma}{E} + 0.002\left(\frac{\sigma}{\sigma_y}\right)^n \tag{12}$$

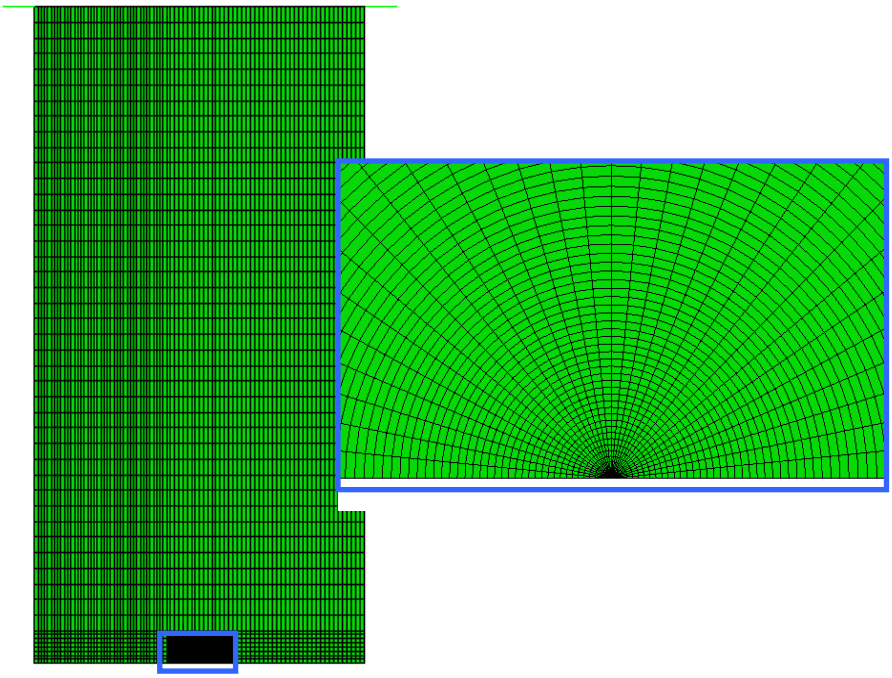

Figure 1. Illustration of Typical Mesh and Fine Detail of Focused Region.

Secondary Loading

To investigate the effects of secondary stress, a through-wall, thermally induced bi-axial bending stress was applied to the DENT, SENT and CCPT geometries with the rigid surface prevented from rotating, i.e. it remains horizontal but can move in the vertical direction. A through wall temperature distribution was used on the basic geometry to create a linear bending stress profile, varying from $+\sigma_b$ to $-\sigma_b$, with a stress of $+\sigma_b$ at the cracked location and a stress of $-\sigma_b$ at the un-cracked surface.

A temperature distribution was applied to SENT, DENT and CCPT models, through use of a user subroutine, to create a temperature distribution through the base geometry from $+T$ to $-T$. This temperature was modified to provide values of σ_b which results in four different magnitudes of secondary reference stress normalised by the material yield stress, σ^s_{ref}/σ_y equal to 0.25, 0.5, 1 and 1.5. The required value of σ_b corresponding to each reference stress was calculated from a simplified limit load solution given in the Miller Compendium of limit loads [8] for an edge cracked plate.

As the bending residual stress field cannot be applied to the SENB model through the same means, as the rigid surface has to be free to rotate and would instantly accommodate the stress, a uniform temperature drop was applied to induce a biaxial tensile residual stress field for the SENB geometry (as can be seen in Figure 1). To allow the stress to be established the rigid surface was prevented from any vertical displacement, i.e. remains in the same position in the Y axis (i.e. vertical axis in Figure 1) but can rotate. The magnitude of the secondary tensile stress applied for the SENB case was chosen to correspond to normalised secondary reference stress values of 0.125, 0.25, 0.5 and 0.75. This reduction was to ensure that excessive plastic deformation, and the associated constraint loss, did not occur before the primary load was applied. The change in temperature for each case was approximately determined as in Equation (13).

$$\Delta T = (1 - a/w)\sigma^s_{ref}/E\alpha \tag{13}$$

Primary Loading

For the SENT, DENT and CCPT cases, the uni-axial primary load was applied as a point load applied to a reference node controlling a rigid surface attached to the top surface of the model. The reference node was constrained from translating and from rotating, ensuring pure tensile stresses were transferred to the model. The lateral surface interaction of the rigid surface and the top of the model was set as frictionless, allowing the model to contract correctly under loading. For the SENB model, the primary load was applied as a bending moment applied to the reference node of the rigid surface. This required the surface interaction to be changed from frictionless to rough so that the model could bend freely without being laterally "ejected" from the rigid surface.

The magnitude of the applied load, P, at the reference node was obtained by an iterative process whereby, initially, a handbook estimate of the limit load, P_L, was used to apply loads corresponding to values of L_r from 0.1 through to 1.6 in increments of 0.1, where $L_r = P/P_L$. This estimate of P_L was then used for all strain hardening coefficients and a group of failure assessment curves established. The estimate of P_L was consequently scaled to ensure that the skeletal point, that is the point at which the FAD is independent of the material's strain hardening, was positioned at $L_r = 1$. This should have provided an improved estimate of the primary reference stress as all hardening curves have the same yield stress and, hence, should have the primary reference stress at $L_r = 1$ as $L_r = \sigma^{p}_{ref} / \sigma_y$. It is noted that the resultant limit load approach adopted was always within 5% of the R6 solution for that geometry under plane strain Mises conditions. The shifts adopted to the limit load to ensure the skeletal point position is at $L_r = 1$ are therefore only within the expected tolerance of handbook solutions. In all cases under combined loading, the primary load was applied after the thermally induced secondary stress.

Determination of the Crack-tip Constraint Correction Terms, Q and β

Estimates of crack-tip constraint are obtained by comparison of the stress field ahead of a cracked component to that obtained, at an equivalent distance, on the MBL model for the same value of J. In this work the distance, *r*, ahead of the crack has been taken as $2J/\sigma_y$, which is common practice. A value for Q has been obtained for all cases considered as summarised by Equation (14).

$$\frac{\sigma_{\theta\theta} - (\sigma_{\theta\theta})_{MBL}}{\sigma_y} = Q \qquad \theta = 0 \qquad r = 2J/\sigma_y \tag{14}$$

where $\sigma_{\theta\theta}$ is the circumferential stress at the radial position defined by θ and $(\sigma_{\theta\theta})_{MBL}$ is the circumferential stress at the radial position defined by θ from the MBL model. The range of analyses performed required that three MBL models were generated for the different strain hardening curves and a large amount of data interpretation performed. This process was made more efficient through the use of python scripts to interrogate the finite element results and macros within the spreadsheets to perform the data interpolation. Values for β were obtained via Q as in Equation (11).

FINITE ELEMENT RESULTS

Estimates of g()$_{FE}$

Figure 2 below provides an example result for the estimate of $g()_{FE}$ for the CCPT geometry with a small crack and small secondary stress. In each of the following figures, the green curves represent the finite element results with a strain hardening of $n = 5$, blue for $n = 7.5$ and red for $n = 10$. Also included in the figures are estimates of $g()$ accounting for the effect of geometric constraint, which is introduced further below. Collectively, it was possible to take the maximum value of $g()_{FE}$ for each strain hardening for each case considered and obtain estimates of the A and B terms that satisfy Equations (8) and (10) as

in [4]. The value for B is simply the skeletal point of $g()_{FE}$ but A has to be fitted. The resulting values for A and B for all cases can be seen in Table 1.

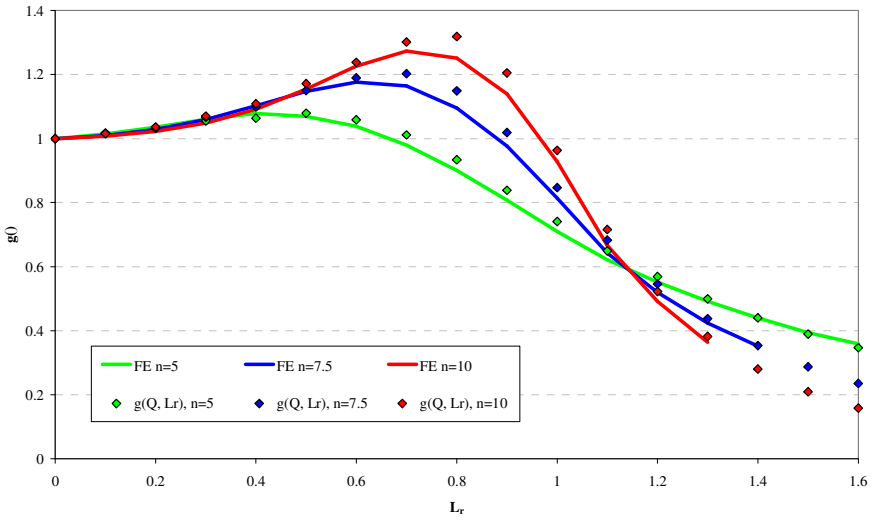

Figure 2. Example of $g()_{FE}$ results and $g(Q, L_r)$ estimate

Table 1. Fit of A and B parameters to $g()_{FE}$.

	Shallow Crack		Deep Crack	
	A	B	A	B
SENT	-0.8	1.10	-0.6	1.15
SENB	-0.6	1.20	-0.8	1.25
DENT	-0.4	1.05	0.2	1.00
CCPT	-1.1	1.10	-0.3	1.08

Estimates of the Constraint Parameters Q and β

The estimates of Q can be seen in Figure 3 for primary loading only. The plot is presented in J - Q space and the same colour convention as above. The symbols used denote the specimen type.

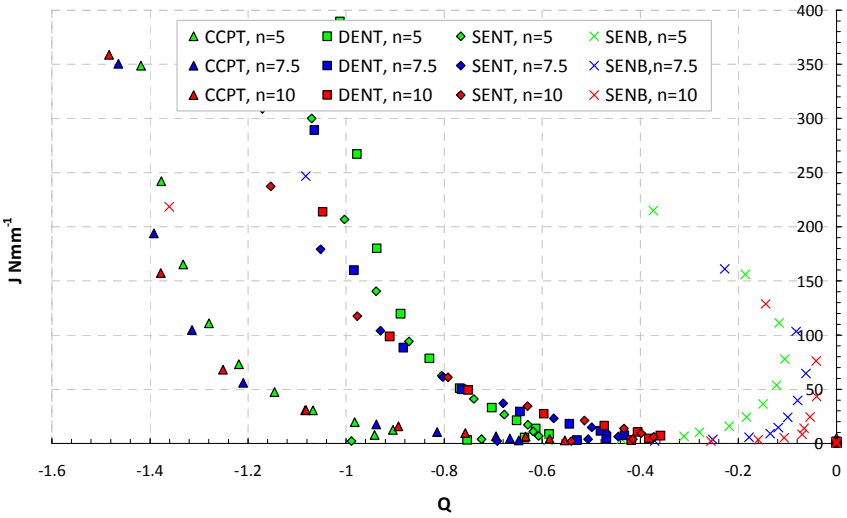

Figure 3. Example of J-Q results for the four specimen types with a long crack and primary loads only

Values for β have been obtained by Equation (11) by normalising Q by L_r. An illustration of β for the results in Figure 3 is shown in Figure 4 where β provides a more constant estimate of constraint.

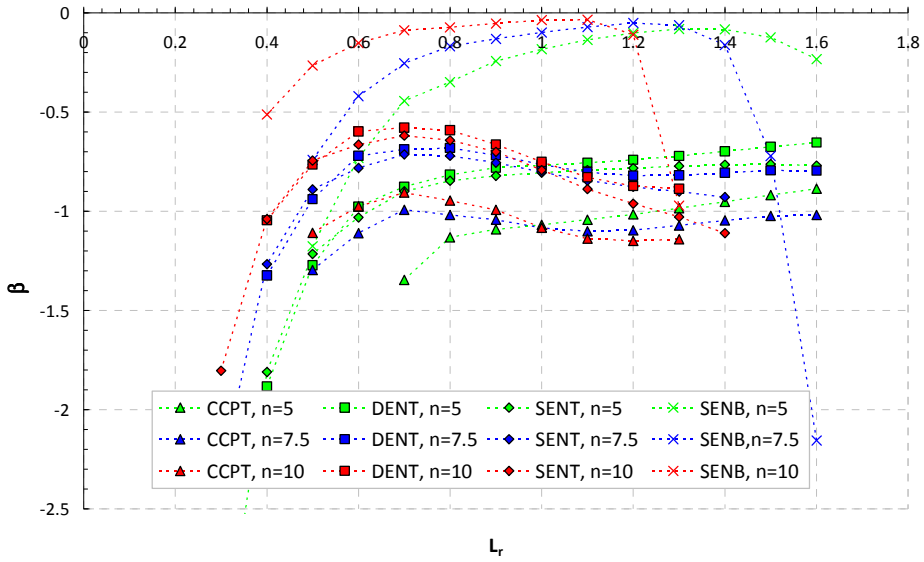

Figure 4. Example of β-L_r results for the four specimen types with a long crack and primary loads only

DISCUSSION

Features of $g()_{FE}$

It was noted that although the trend in results was the same as observed in [4], the effect of the secondary stress is more significant than before, where the enhancement was essentially independent of the magnitude of the secondary stress. However, it was noted that the SENT specimen shows the least variation of all geometries and it is this geometry which is closest to the external circumferentially cracked cylinder used in [4]. In all cases, it was the lowest magnitude of secondary stress which has the highest increase in $g()_{FE}$.

The values of A and B, obtained from $g()_{FE}$, have been shown in Table 1and are, in general, seen to follow the conservative estimates in [4]; that A can be taken as -0.8 and B as 1.25. Of all the cases, only the shallow cracked CCPT specimen fails to comply with this as a value of A of -1.1 is shown. It is also noted that the deeper cracked specimens have a larger value of A (i.e. less negative) indicating that another feature, such as constraint or geometric effects, is also having an effect. It is also noted that the curve fit of the SENB results through modifying A and B is not very good. This may be because the purely tensile secondary stress adopted could be considered as acting more like a primary stress and may require approached adopting estimates of elastic follow-up [2, 3].

Crack Tip Constraint

The estimates of Q in Figure 3 for all geometries under pure primary loads show that the geometry has a much more significant effect on crack-tip constraint than the material's strain hardening, which would be expected. It is also clear that the CCPT specimen has the lowest (most negative) value of Q, ahead of the SENT and DENT specimens, which have similar estimates of Q, and the SENB specimen which has the highest value of Q. It was also noted that the shallower crack has a lower value of Q than the deeper crack. All these results are what would normally be expected and help to confirm that the estimates are accurate, in terms of geometric and material behaviour at least. Although not presented in this paper (for reasons of brevity) the addition of secondary stress was noted to demonstrate a

couple of features: 1) the magnitude of secondary stress only had a minor influence on the results; and 2) compared to the cases which have only a primary load applied, the secondary stress cases generally shifted the value of Q to the right (i.e. tending to become more positive). This would be expected as the applied secondary stress is a bending stress and should increase constraint. Likewise, the shallow crack will not experience such a strong bending field ahead of the crack tip, and, as such, does not demonstrate as much of a shift.

Figure 4 shows the behaviour of β against L_r under primary loads alone. It can be seen that β remains reasonably constant between $L_r = 0.6$ and $L_r = 1.4$. This region incorporates the small-scale yielding zone in which the enhancement of $g()$ is most prominent. Below $L_r = 0.6$, the estimates of Q, and hence β, became harder to accurately obtain within the interpolation spreadsheets used for this analyses. Above $L_r = 1.2$, the estimates of J become questionable so that the estimates of Q have greater errors associated with them. It is therefore the level region of β against L_r which has been assumed to be a representative value of β for that case.

g() as a function of L_r and Constraint, g(Q, L_r)

The values of β plotted in Figure 4, when L_r is above approximately 0.5, can be seen to be approximately -0.6 to -0.8 for the SENT and DENT geometries and about -1 to -1.2 for the CCPT case. It is noted that these are similar to the values of A presented in Table 1. This has led to the concept that the β term could be used in place of A in defining $g()$ in Equation (8) so that a version of $g()$ can be defined which incorporates constraint, $g(Q, L_r)$, as:

$$g(Q, L_r) = \left[\frac{E\varepsilon_{ref}^{mod}}{\sigma_{ref}^{mod}} + \frac{\beta\left(\sigma_{ref}^{mod} / \sigma_y\right)^2}{E\varepsilon_{ref}^{mod} / \sigma_{ref}^{mod}} \right]^{-1/2} \tag{15}$$

Figure 2 includes an example result when adopting this estimate of $g(Q, L_r)$. The particular case in Figure 2 shows reasonable agreement. Generally, however, it was noted that this prediction was more accurate for the lowest secondary stress and became conservative for larger secondary stresses (which may have self-induced plastic strains). For the smaller secondary stress, good agreement was observed for most cases with a very good match for the shallow cracked CCPT and SENT, and the deeply cracked SENT, specimens. The SENB specimens were poorly fitted by $g(Q, L_r)$, although it was only the deeply cracked case which was non-conservative, and may be a result of elastic follow-up as discussed above.

It is noted that the use of $g(Q, L_r)$ to provide estimates of the combined crack driving force should provide an estimate of J which is less conservative than that contained currently in R6. It is considered that, when performing a constraint analyses, this will not remove the need to correct the material's fracture toughness, and, as such, should not change the methodology outlined in R6 for dealing with constraint. However, it is still considered prudent to reconsider this in more detail.

In most cases Equations (8), (9) and (10) provide a conservative estimate of $g()$. However, it is noted that the CCPT geometry with a shallow crack might be non-conservative as the value of A required to fit the data is less (i.e. more negative) than -0.8 and for some geometries the required value of A is larger than -0.8 (i.e. more positive), meaning Equation (8) might be overly conservative. The work therefore indicates that the enhancement to the secondary stress contribution is related to the ease (and magnitude) to which the plastic zone develops before redistribution effects dominate. However, occasions where the estimate of $g()$ might be considered as potentially non-conservative are inherently the cases which include the most conservatism in the overall assessment through constraint loss. Conversely if constraint loss is invoked, it may be necessary to adopt such an approach as suggested here.

Comparisons of g(), g(Q, L_r) and the R6 ξ Factor

To provide further comparison of the previously defined $g()$, as in Equation (8) to (10), $g(L_r, Q)$ and an estimate from R6 based on the ξ factor have also been normalised by $g()_{FE}$ and plotted against L_r. An example result is shown in Figure 5. A 10% error margin either side of the 1:1 equivalent line has been adopted, where the 10% error margin is taken as the potential errors associated with the comparison of the GE-EPRI handbook solutions for K_J and the finite element analyses. The estimates of $g()$ are shown as coloured diamonds, the estimates of $g(L_r, Q)$ are shown as solid lines and the R6 estimate is shown as dashed lines. The R6 estimate has been based on the ξ factor shown in Equation (6) and has been divided by $f_1(L_r)$ to allow the comparison to be equivalent to g as shown in Equation (7), where $f_1(L_r)$ represents the Option 1 FAD of Equation (3). These results showed that the current R6 estimate of $g()$, defined by $\xi / f(L_r)$, is very conservative for all cases, always increasing well above $2\, g()_{FE}$. However, it is noted that this magnitude of error will not necessarily reflect such large conservatism in the estimates of K_J as it is often the primary contribution which is dominant at these values of L_r. These plots show only minor differences between the $g()$ defined in Equation (8) to (10) and $g(Q, L_r)$; with $g(Q, L_r)$ generally being slightly closer to the 1:1 line. That both $g()$ and $g(Q, L_r)$ nearly always remain within the ±10% margin helps provide further confidence in both approaches. These comparisons help show that the constraint modified approach can help improve the estimates of $g()$ over those in Equation (8) to (10) but in most cases is only of minimal benefit. However, these plots do help demonstrate the observed conservatisms in R6 and that the $g()$ approach is potentially more accurate.

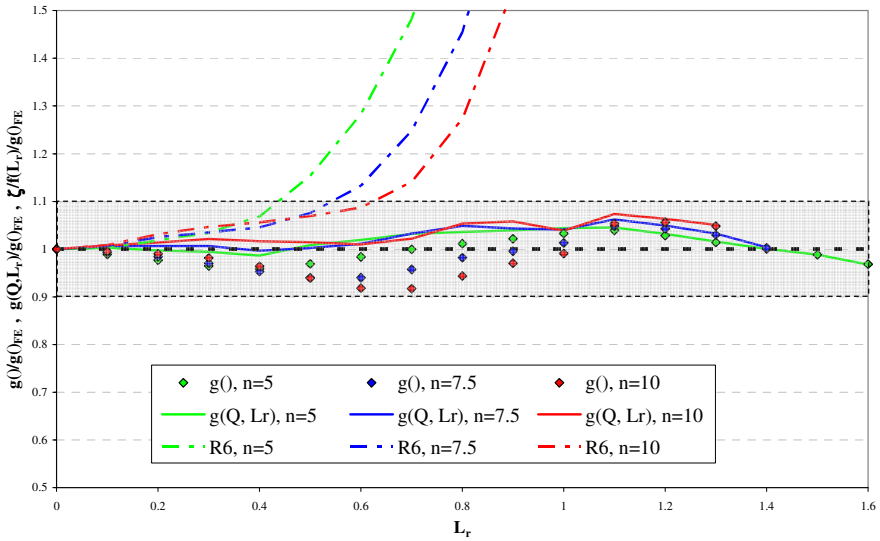

Figure 5. Estimates of *g()* normalised by the FE value for a shallow cracked CCPT specimen

CONCLUSIONS

The work has considered a range of geometries that exhibit different levels of constraint with the primary aim of providing further confidence in the use of $g()$ and a secondary aim of investigating a potential link between $g()$ and the crack-tip constraint parameter, Q. This has necessitated a large range of detailed finite element analyses to determine both $g()$ and Q. The work has shown that the previously

provided estimate of $g()$ is suitable for almost all the scenarios considered in this paper and that it is possible to provide an improved estimate by taking account of constraint which has led to an initial estimate of $g(Q, L_r)$. The conclusions made are as follows:

- The estimates of $g()_{FE}$ considered in this paper follow the same trends and results as Equation (8), reflecting those previously presented in [4], and provide further confidence in the methodology.
- The work therefore indicates that occasions where the estimate of $g()$ might be considered as potentially non-conservative are inherently the cases which include the most conservatism in the overall assessment through constraint loss. Conversely if constraint loss is invoked, it may be necessary to adopt the approach suggested here.
- Estimates of crack-tip constraint level by using the $\beta = Q/L_r$ parameter is more useful here as it shows little variation with applied load.
- Using the β term instead of the A term in $g(Q, L_r)$ shows promise as it captures the enhanced $g()$ for the CCPT geometry, accurately predicts $g()$ for the SENT geometry and captures the reduction in $g()$ for the DENT geometry.
- In real terms, this benefit may be small compared to estimates of $g()$ from Equations (8), (9) and (10). Both $g()$ and $g(Q, L_r)$ have shown improved comparisons to the finite element analyses compared to an equivalent estimate from R6.

ACKNOWLEDGEMENTS
This paper is published with the permission of AMEC and EDF Energy. The work was performed as part of the development programme for the EDF Energy R6 procedure.

REFERENCES

1 - R6, Revision 4: Assessment of the Integrity of Structures Containing Defects, EDF Energy, 2011.
2 - Song, T.K., Kim, Y.J., Ainsworth, R.A., and Nikbin, K.M., "Approximate J estimates for combined primary and secondary stresses with large elastic follow-up", International Journal of Pressure Vessels and Piping, 2012, under review.
3 - Ainsworth, R.A., "Consideration of elastic follow-up in the treatment of combined primary and secondary stresses in fracture assessments", Engineering Fracture Mechanics, vol. 96, pp 558-569, 2012.
4 - James, P.M., Hooton, D.G., Madew, C.J. and Sherry, A.H., "Predictions of elastic-plastic crack driving force and redistribution under combined primary and secondary stresses – Part 1: Analytical investigation", International Journal of Pressure Vessels and Piping, vol. 101, pp 101-112, 2013.
5 - James, P.M., Hutchinson, P., Madew, C.J. and Sherry, A.H., "Predictions of elastic-plastic crack driving force and redistribution under combined primary and secondary stresses – Part 2: Experimental application", International Journal of Pressure Vessels and Piping, vol. 101, pp 91-100, 2013.
6 - Ainsworth, R.A., "A Constraint-Based Failure Assessment Diagram for Fracture Assessment", International Journal of Pressure Vessels and Piping, 64, 277-285, 1995.
7 - ABAQUS Version 6.9, ABAQUS inc., 2009.
8 - Miller, A.G., "Review of Limit Loads of Structures Containing Defects", Int. J of Pressure Vessels and Piping, 32 (1988), 197-327.